Electrocatalysis

DOI: 10.1002/ange.201205022

Hydroxide Ion Conducting Antimony(V)-Doped Tin Pyrophosphate Electrolyte for Intermediate-Temperature Alkaline Fuel Cells**

Takashi Hibino, Yanbai Shen, Masakazu Nishida, and Masahiro Nagao*

Alkaline fuel cells have received significant interest in recent years relative to acid fuel cells, because of advantages when operating under alkaline conditions, which include enhancement of the electrode reaction kinetics, especially at the cathode, as the cathode catalyst is not subjected to corrosion.[1] Consequently, non-noble metals or inexpensive metal oxides can be used as catalysts.[2] In addition, high energy density liquids and gases such as ethanol, hydrazine, and ammonia can be adopted as fuels.[3] Anion exchange polymers are widely viewed as promising candidates for electrolyte membranes; however, a major challenge in the development of such polymers is their stability at high pH,[4] because both the main chain and functional groups are easily degraded by hydroxide ion attacks. In addition, the poor chemical stability of current anion exchange polymers means that the operating temperature is limited to 80 °C or less; therefore, this type fuel cell is typically operated between 50 and 60 °C.[5]

Operating a fuel cell at elevated temperatures provides the anode catalyst with high tolerance to CO, which is useful for both acid and alkaline fuel cells.[6] Additional benefits include small polarization loss, good drainage at the anode, and effective heat dissipation from the fuel cell system. A few anion-conducting electrolyte materials capable of operating at intermediate temperatures (100–200 °C) have been reported, such as KOH-doped polybenzimidazole (PBI)[6] and hydroxide ion-intercalated Mg–Al layered double hydroxide (LDH).[7] However, the reaction of KOH in the former electrolyte with CO_2 present in the air to form K_2CO_3 is a possibility, and the hydroxide ion conductivity of the latter (0.03 $S\,cm^{-1}$ at 200 °C) is not sufficiently high to achieve satisfactory cell performance. Further increases in chemical stability and conductivity would enhance the position of intermediate-temperature anion exchange membranes as the preferred electrolyte material for practical alkaline fuel cells.

In this study, metal pyrophosphates (MP_2O_7) were studied as anion-conducting electrolytes for intermediate temperature applications. The metal pyrophosphate structure can be described as a network of MO_6 octahedra sharing corners with P_2O_7 units, characterized by the presence of intersecting zigzag tunnels delimited by pentagonal windows.[8] This unique crystalline structure provides many ion exchange sites and transport pathways. To date, proton exchange capability is typically introduced into the bulk of SnP_2O_7 by the partial substitution of Sn^{4+} cations with low-valency cations, such as In^{3+}, Al^{3+}, Mg^{2+}, Sb^{3+}, Sc^{3+}, Ga^{3+}, and Zn^{2+}.[9] The resultant proton conductivity reaches approximately 0.1 $S\,cm^{-1}$ at 200 °C.[10] An opposite effect is expected by the partial substitution of Sn^{4+} cations with high-valency cations, which would result in hydroxide ion exchange capability because of charge compensation for the high-valency cations. We demonstrate the hydroxide ion conduction of pentavalent cation-doped SnP_2O_7 at intermediate temperatures using electrochemical measurements, including complex impedance, gas concentration cells, and H/D isotope replacement methods. Moreover, $Sn_{0.92}Sb_{0.08}P_2O_7$, which exhibits the highest hydroxide ion conductivity among the tested compounds, is characterized with respect to the hydroxide ion environment and the basicity of the compound. In addition, fuel cell tests with the $Sn_{0.92}Sb_{0.08}P_2O_7$ electrolyte were conducted in the temperature range of 50–200 °C.

The crystalline structure of Sb^{5+}-doped SnP_2O_7 as an example of $Sn_{1-x}A_xP_2O_7$ (A^V = pentavalent cation dopants) was identified using X-ray diffraction (XRD) measurement (see Figure S1 in the Supporting Information). The XRD pattern of the nondoped sample was assigned to SnP_2O_7 (72 mol %) and SnO_2 (28 mol %). Tao interpreted the presence of the SnO_2 phase to be due to the use of large SnO_2 particles as a raw material, which causes the formation of a core–shell structure,[9c] although such a structure could not be determined from transmission electron microscopy (TEM) measurements (see Figure S2 in the Supporting Information). (The content of SnO_2, which has a negative effect on ionic conduction, can be reduced when smaller SnO_2 particles are used as a raw material.) $Sn_{1-x}Sb_xP_2O_7$ with an Sb^{5+} content of not more than 8 mol % had the same pattern as that of the nondoped sample. The peaks attributable to SnP_2O_7 were shifted slightly toward higher Bragg angles by an increase in the Sb^{5+} content, which is expected with substitution of Sn^{4+} (0.69 Å) with Sb^{5+} (0.60 Å) of a smaller ionic radius.[11] As a consequence, the lattice constant of SnP_2O_7 decreased from 7.925 to 7.916 Å with increasing Sb^{5+} content from zero to 8 mol %. In contrast, $Sn_{1-x}Sb_xP_2O_7$ with an Sb^{5+} content of 10 mol % or higher contained some peaks attributable to $Sn_{2.5}P_3O_{12}$, which indicates that 8 mol % Sb^{5+} is the substitution limit.

The temperature dependency of the electrical conductivity for $Sn_{1-x}Sb_xP_2O_7$ was measured in air saturated with H_2O vapor at 50 °C (Figure 1) and revealed two common features.

[*] Prof. Dr. T. Hibino, Dr. Y. Shen, Dr. M. Nagao
Graduate School of Environmental Studies, Nagoya University
Nagoya 464-8601 (Japan)
E-mail: hibino@urban.env.nagoya-u.ac.jp
M. Nishida
Research Institute Instrumentation Frontier
National Institute of Advanced Industrial Science and Technology
Nagoya 463-8560 (Japan)

[**] This work was supported by KAKENHI (grant number 21350073).

Supporting information for this article is available on the WWW under http://dx.doi.org/10.1002/anie.201205022.

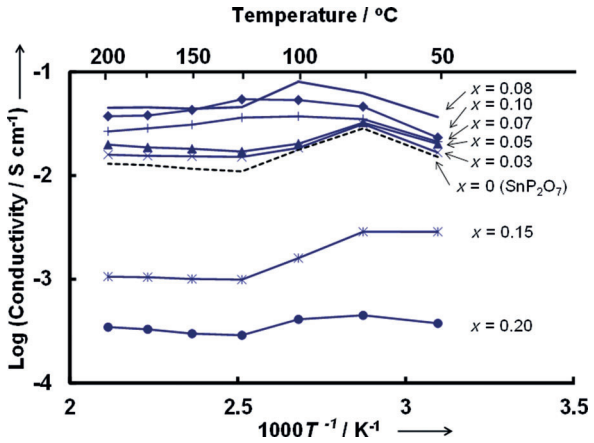

Figure 1. Temperature dependence of the conductivity for $Sn_{1-x}Sb_xP_2O_7$ ($x = 0$–0.2).

Firstly, the electrical conductivity for all the tested samples except $Sn_{0.85}Sb_{0.15}P_2O_7$ initially increased and then decreased with increasing temperature, and the temperature of maximum electrical conductivity was dependent on the Sb^{5+} content. Secondly, the electrical conductivity increased with increasing Sb^{5+} content and reached a maximum at an Sb^{5+} concentration of 8 mol%, which corresponds well with the substitution limit for Sb^{5+} estimated from XRD measurements. ($Sn_{2.5}P_3O_{12}$ was formed as an impurity when the Sb^{5+}content was ≥ 8 mol%; see Figure S1 in the Supporting Information.) Therefore, it is possible that such an impurity interrupts the hydroxide ion transfer between $Sn_{1-x}Sb_xP_2O_7$ particles. These results support that the doping of pentavalent cations plays an important role in the appearance of hydroxide ion conduction. As a result, $Sn_{0.92}Sb_{0.08}P_2O_7$ exhibited the highest electrical conductivity over the temperature range tested; 0.08 S cm^{-1} at 100 °C and 0.05 S cm^{-1} at 200 °C. Note that the electrical conductivity is further enhanced by an increase in the H_2O vapor concentration; an electrical conductivity of 0.07 S cm^{-1} at 200 °C was obtained when the air was saturated with H_2O vapor at 70 °C.

An effect similar to that of Sb^{5+} doping was expected for other pentavalent cations. Therefore, $Sn_{0.92}V_{0.08}P_2O_7$, $Sn_{0.92}Nb_{0.08}P_2O_7$, and $Sn_{0.92}Ta_{0.08}P_2O_7$ were also synthesized. These samples were indexed with a crystalline structure similar to that of $Sn_{0.92}Sb_{0.08}P_2O_7$, although $Sn_{0.92}Ta_{0.08}P_2O_7$ contained a $Ta_2P_3O_{12.5}$ impurity phase. Significant enhancement of the electrical conductivity was observed for all the doped samples. The order of electrical conductivity was ($Sn_{0.92}Sb_{0.08}P_2O_7 >$) $Sn_{0.92}Nb_{0.08}P_2O_7 > Sn_{0.92}V_{0.08}P_2O_7 > Sn_{0.92}Ta_{0.08}P_2O_7$ ($> SnP_2O_7$). The relatively low electrical conductivity of $Sn_{0.92}Ta_{0.08}P_2O_7$ is probably due to the presence of the impurity phase. In contrast, the tetravalent cation-doped SnP_2O_7 (dopant = Si^{4+} and Ce^{4+}) compounds had comparable or lower electrical conductivities than that of nondoped SnP_2O_7, which supports the effect of pentavalent cation doping on the electrical conductivity. These results confirm the validity of this approach to the design of hydroxide ion-conducting materials. $Sn_{0.92}Sb_{0.08}P_2O_7$ was used as the test sample for subsequent experiments.

The common valence states of antimony are Sb^{3+} and Sb^{5+}, which were clarified by X-ray photoelectron spectroscopy (XPS) analysis of $Sn_{0.92}Sb_{0.08}P_2O_7$. The binding energy of antimony in $Sn_{0.92}Sb_{0.08}P_2O_7$ was found to be 542.2 eV, which corresponds to Sb^{5+} $3d_{3/2}$. (The binding energy reported for Sb^{3+} $3d_{3/2}$ is about 539 eV.[12]) Therefore, it was confirmed that at least all of the antimony present on the sample surface was Sb^{5+}.

The thermogravimetric analysis (TGA) curve of $Sn_{0.92}Sb_{0.08}P_2O_7$ indicated that a weight loss of about 4% occurred in two steps between 50 and 400 °C, accompanied by endothermic peaks at approximately 80 and 165 °C in the differential thermal analysis (DTA) profile. The two endothermic peaks can be ascribed to the desorption of physisorbed and chemisorbed water molecules, because these peaks were also observed for nondoped SnP_2O_7.

Thus, the dehydration of hydroxide ions that are assumed to be incorporated into $Sn_{0.92}Sb_{0.08}P_2O_7$ does not occur until at least 400 °C. This is reflected in the high electrical conductivity of 0.03 S cm^{-1} for this sample, even at 300 °C.

The microstructure of $Sn_{0.92}Sb_{0.08}P_2O_7$ was investigated using Fourier transform infrared (FT-IR) spectroscopy. $Sn_{0.92}Sb_{0.08}P_2O_7$ has a distinctive structure characterized by three absorption bands assigned to an OH stretching vibration centered at 3375 cm^{-1}, XOH bending vibrations centered at 2820 and 2330 cm^{-1}, and an OH bending vibration centered at 1650 cm^{-1} (Figure 2).[13] The intensity of these bands was

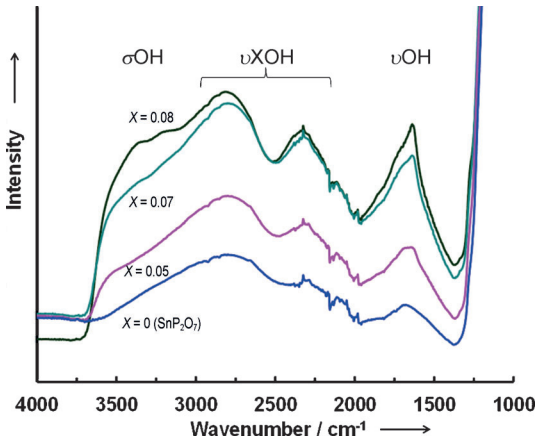

Figure 2. FT-IR spectra for $Sn_{1-x}Sb_xP_2O_7$ ($x = 0$, 0.05, 0.07, and 0.08).

enhanced by an increase in the Sb^{5+} content. While care was taken to account for water molecules adsorbed on the sample surface, the results suggest that the absorption bands are mainly attributable to hydroxide ions present in the bulk and on the surface of $Sn_{0.92}Sb_{0.08}P_2O_7$.

If $Sn_{0.92}Sb_{0.08}P_2O_7$ has anion exchange capability, then hydroxide ions can be replaced with other anions, such as chloride and bromide ions. The $Sn_{0.92}Sb_{0.08}P_2O_7$ sample powder was added to 1M KCl or KBr solution and stirred magnetically at room temperature overnight. The electrical conductivity of the obtained samples was four or five orders of magnitude lower than that of the untreated sample over the tested temperature range (see Figure S3 in the Supporting

Information). The transport of hydroxide ions exhibits Grotthuss behavior in these anion exchange membranes, where hydroxide ions are naturally integrated into the hydrogen-bonding network of water molecules.[14] However, this mechanism is not applicable to chloride and bromide ion-exchanged samples, which exhibit significantly low ion conductivities.

To gain further insight into the hydroxide ion conduction in $Sn_{0.92}Sb_{0.08}P_2O_7$, several characteristics were compared with proton-conducting $Sn_{0.9}In_{0.1}P_2O_7$. The acidity and basicity of both samples were measured using NH_3- and CO_2-desorption (TPD) methods, respectively. In the NH_3 desorption profiles, both samples had two major desorption peaks in the temperature ranges of 150–250 °C and 250–450 °C (see Figure S4a in the Supporting Information); the peak that appears in the low-temperature region is caused by physisorbed and weakly chemisorbed NH_3, and the peak that appears in the high-temperature region is associated with Brönsted acid sites.[15] Both peaks were much smaller for $Sn_{0.92}Sb_{0.08}P_2O_7$ than for $Sn_{0.9}In_{0.1}P_2O_7$, and considering the similar surface areas of the samples, this result indicates that the acidity of $Sn_{0.92}Sb_{0.08}P_2O_7$ is weaker than that of $Sn_{0.9}In_{0.1}P_2O_7$ (Figure 3). On the other hand, the CO_2 desorption profiles had small and broad peaks between 50 and 200 °C for both samples; however, the intensity for $Sn_{0.92}Sb_{0.08}P_2O_7$ was somewhat higher than that for $Sn_{0.9}In_{0.1}P_2O_7$ (Figure S4b in the Supporting Information). More importantly, only $Sn_{0.92}Sb_{0.08}P_2O_7$ had a relatively large peak between 450 and 530 °C. Although identification of these peaks still remains unclear at the present time, it is reasonable to conclude that the basicity of $Sn_{0.92}Sb_{0.08}P_2O_7$ is higher than that of $Sn_{0.9}In_{0.1}P_2O_7$.

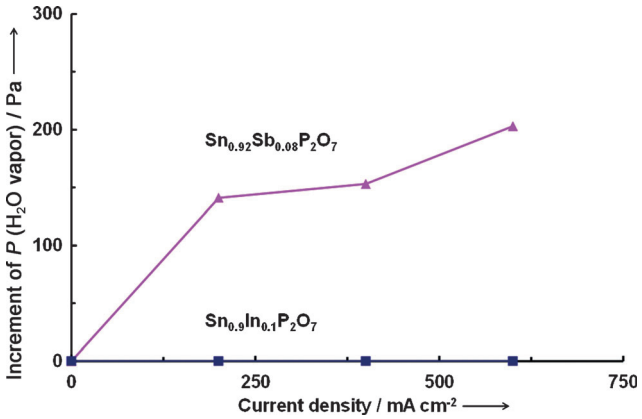

Figure 3. Increment of $P(H_2O)$ in the outlet gas from the anode chamber for fuel cells with $Sn_{0.92}Sb_{0.08}P_2O_7$ and $Sn_{0.9}In_{0.1}P_2O_7$ electrolytes.

Ionic conduction in $Sn_{0.92}Sb_{0.08}P_2O_7$ and $Sn_{0.9}In_{0.1}P_2O_7$ was investigated by fabricating a steam gas concentration cell using the sample pellets as electrolytes. In the case of the proton conductors, the following reactions occur by the partial pressure gradient of H_2O vapor between the two electrodes [Eqs. (1) and (2); $P(H_2O)$ = water pressure]:

$$\text{Electrode at the high } P(H_2O) \text{ side}: \quad H_2O \rightarrow 2H^+ + 2e^- + 1/2\,O_2 \tag{1}$$

$$\text{Electrode at the low } P(H_2O) \text{ side}: \quad 1/2\,O_2 + 2H^+ + 2e^- \rightarrow H_2O \tag{2}$$

The resultant potential of the electrode at the high $P(H_2O)$ side becomes negative against the electrode at the low $P(H_2O)$ side. In the case of the hydroxide ion conductors, the following reactions are proposed [Eqs. (3) and (4)]:

$$\text{Electrode at the high } P(H_2O) \text{ side}: \quad H_2O + 1/2\,O_2 + 2e^- \rightarrow 2OH^- \tag{3}$$

$$\text{Electrode at the low } P(H_2O) \text{ side}: \quad 2OH^- \rightarrow H_2O + 1/2\,O_2 + 2e^- \tag{4}$$

These reactions cause an opposite polarity to that for the proton conductors, so that the potential of the electrode at the high $P(H_2O)$ side becomes positive against the electrode at the low $P(H_2O)$ side.[16] As expected, the galvanic cell with $Sn_{0.9}In_{0.1}P_2O_7$ generated negative electromotive forces (EMFs), and the galvanic cell with the $Sn_{0.92}Sb_{0.08}P_2O_7$ had inverse behavior (Figure S5 in the Supporting Information).

The H/D isotope effect on the electrical conductivity is helpful to develop a more detailed understanding of the ionic conduction in $Sn_{0.92}Sb_{0.08}P_2O_7$ and $Sn_{0.9}In_{0.1}P_2O_7$. The electrical conductivity of $Sn_{0.9}In_{0.1}P_2O_7$ was reduced by replacing H_2O vapor with D_2O vapor (Figure S6 in the Supporting Information), which confirms that protons function as the charge carrier in this sample.[17] In contrast, the behavior observed for $Sn_{0.92}Sb_{0.08}P_2O_7$ was complicated; the H/D isotope effect was observed at 50 and 75 °C, but disappeared at 100 °C or higher temperatures (Figure S6 in the Supporting Information), which suggests that proton conduction is dominant at temperatures below 100 °C, but that hydroxide ion conduction is significant at 100 °C or higher. This complicated phenomenon can be interpreted as a consequence of an additional transport pathway for protons at low temperatures. The sample was exposed to air saturated with H_2O vapor at 50 °C; therefore, the relative humidity becomes higher as the temperature is decreased. As a result, the adsorption of excess H_2O vapor on the surface of the sample powder produces transport pathways for protons. However, these pathways are lost by an increase in temperature, so that hydroxide ion conduction becomes predominant over proton conduction at high temperatures.

More direct evidence is required to support the hydroxide ion conduction of $Sn_{0.92}Sb_{0.08}P_2O_7$, especially at 100 °C or higher. H_2O vapor is generally produced at the anode for hydroxide ion-conducting fuel cells, and at the cathode for proton-conducting fuel cells. This phenomenon was verified for $Sn_{0.92}Sb_{0.08}P_2O_7$ and $Sn_{0.9}In_{0.1}P_2O_7$ by experiments conducted at 200 °C, at which a large quantity of current could be drawn from the fuel cell, as described later. No H_2O vapor product was observed at the anode for the fuel cell with the $Sn_{0.9}In_{0.1}P_2O_7$ electrolyte during cell operation, whereas the partial pressure of H_2O vapor in the outlet gas from the anode chamber increased with current density for the fuel cell with

$Sn_{0.92}Sb_{0.08}P_2O_7$ (Figure 3). Although it is difficult to quantitatively analyze the experimental data obtained from the low sensitivity hydrometer, this result demonstrates that $Sn_{0.92}Sb_{0.02}P_2O_7$ functions as a hydroxide ion conductor under the operation conditions employed, where the hydrogen oxidation reaction proceeds through Reaction (5):

$$\text{Anode}: \quad H_2 + 2\,OH^- \rightarrow 2\,H_2O + 2\,e^- \qquad (5)$$

This investigation has confirmed that hydroxide ions migrate in the bulk and on the surface of $Sn_{0.92}Sb_{0.08}P_2O_7$, especially at 100 °C or higher, which is a large advantage over conventional anion exchange polymers. Therefore, this compound is suitable as an electrolyte material for an intermediate-temperature alkaline fuel cell. Current–voltage (*I-V*) and current–power (*I-P*) characteristics were measured for a fuel cell fabricated with the $Sn_{0.92}Sb_{0.08}P_2O_7$ electrolyte in the temperature range of 75–200 °C. Two particularly noteworthy features were determined from these characteristics (Figure 4). One feature is that the open-circuit voltages (OCVs) at all the tested temperatures were between 950 and

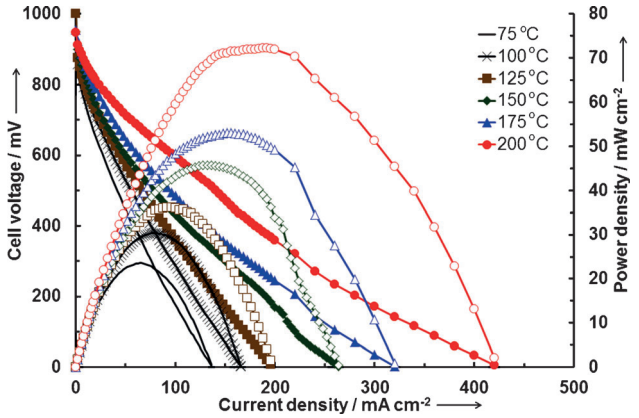

Figure 4. Cell voltage and power density as a function of current density for a fuel cell with the $Sn_{0.92}Sb_{0.08}P_2O_7$ electrolyte. The thickness of the electrolytes was about 1.0 mm.

1000 mV, which is lower than the theoretical value of about 1.1 V. The low OCVs are attributed to the physical leakage of gas through the electrolyte, because the OCVs increased with increasing electrolyte thickness. The other feature is that the voltage drop became smaller at each current density as the temperature increased, the effect of which was large, especially at 150 °C or higher. The resultant power density reached a maximum at 200 °C.

The internal resistances of the fuel cell were analyzed using impedance spectroscopy. The resistance at all tested temperatures was comprised of three components; ohmic, polarization, and diffusion resistance (Figure S7 in the Supporting Information). The ohmic resistance of the electrolyte was between 1.0 and 1.8 $\Omega\,cm^2$ and was dependent on the temperature, which is consistent with the electrical conductivity results (Figure 1). In contrast, the polarization and diffusion resistances were significantly affected by the temperature, and were considerably large, especially at 125 °C or lower. This can be explained by the transition of the charge carrier species in $Sn_{0.92}Sb_{0.08}P_2O_7$, because this material is considered to transform from proton conductor to hydroxide ion conductor with increase in the temperature. In addition, the cathode exhibits low electrocatalytic activity for the oxygen reduction reaction (ORR) under acid conditions, which causes large polarization and diffusion resistances. However, the electrocatalytic activity of this electrode for the ORR is significantly improved under alkaline conditions, which reduces the polarization and diffusion resistances. It should be noted that the electrode properties obtained at 200 °C were substantially larger than those reported for alkaline fuel cells at low temperatures. The low electrode performance is due to the lack of hydroxide ion conduction in the entire cathode, because no ionomer was used in the cathode. Another consideration is that the electrode was only in physical contact with the electrolyte, which probably resulted in a poor electrolyte/electrode interface. Therefore, research is in progress to design a composite electrode based on Pt/C and $Sn_{0.92}Sb_{0.08}P_2O_7$ to improve both the hydroxide ion conduction in the cathode and the electrolyte/electrode interface properties.

In summary, a series of $Sn_{1-x}A_xP_2O_7$ (A^V = V, Nb, Ta, and Sb) compounds were synthesized, of which $Sn_{0.92}Sb_{0.08}P_2O_7$ exhibited the highest electrical conductivity in the temperature range of 50–200 °C. The anion exchange capability of this compound was evaluated using spectroscopic and electrochemical analyses. The experimental results led to the following conclusions. Hydroxide ions are incorporated into the compound by charge compensation for the high valency cation dopants; hydroxide ion conduction is predominant, especially at temperatures of 100 °C and higher. These conclusions are also supported by the intermediate temperature performance of a fuel cell constructed with the $Sn_{0.92}Sb_{0.08}P_2O_7$ electrolyte.

Received: June 27, 2012
Revised: September 5, 2012
Published online: September 26, 2012

Keywords: electrocatalysis · electrochemistry · fuel cells · hydroxide ion conduction · metal pyrophosphates

[1] a) J. R. Varcoe, R. C. T. Slade, *Fuel Cells* **2005**, *5*, 187–200; b) G. Merle, M. Wessling, K. Nijmeijer, *J. Membr. Sci.* **2011**, *377*, 1–35.
[2] a) J. R. Varcoe, R. C. T. Slade, G. L. Wright, Y. L. Chen, *J. Phys. Chem. B* **2006**, *110*, 21041–21049; b) X. Wu, K. Scott, *J. Power Sources* **2012**, *206*, 14–19.
[3] a) K. Asazawa, K. Yamada, H. Tanaka, A. Oka, M. Taniguchi, T. Kobayashi, *Angew. Chem.* **2007**, *119*, 8170–8173; *Angew. Chem. Int. Ed.* **2007**, *46*, 8024–8027; b) E. E. Switzer, T. S. Olson, A. K. Datye, P. Atanassov, M. R. Hibbs, C. J. Cornelius, *Electrochim. Acta* **2009**, *54*, 989–995.
[4] a) P. Hinksman, D. H. Isaac, P. Morrissey, *Polym. Degrad. Stab.* **2000**, *68*, 299–305; b) S. Chempath, J. M. Boncella, L. R. Pratt, N. Henson, B. S. Pivovar, *J. Phys. Chem. C* **2010**, *114*, 11977–11983.
[5] a) S. Gu, R. Cai, T. Luo, Z. Chen, M. Sun, Y. Liu, G. He, Y. Yan, *Angew. Chem.* **2009**, *121*, 6621–6624; *Angew. Chem. Int. Ed.*

2009, *48*, 6499 – 6502; b) H. Zarrin, J. Wu, M. Fowler, Z. W. Chen, *J. Membr. Sci.* **2012**, *394 – 395*, 193 – 201.
[6] J. H. Jiang, T. Aulich, *J. Power Sources* **2012**, *209*, 189 – 194.
[7] H. S. Kim, Y. Yamazaki, J. D. Kim, T. Kudo, I. Honma, *Solid State Ionics* **2010**, *181*, 883 – 888.
[8] P. K. B. Gover, N. D. Withers, S. Allen, R. L. Withers, J. S. O. Evans, *J. Solid State Chem.* **2002**, *166*, 42 – 48.
[9] a) M. Nagao, A. Takeuchi, P. Heo, T. Hibino, M. Sano, A. Tomita, *Electrochem. Solid-State Lett.* **2006**, *9*, A105 – A109; b) X. L. Chen, C. S. Wang, E. A. Payzant, C. R. Xia, D. Chu, *J. Electrochem. Soc.* **2008**, *155*, B1264 – B1269; c) S. W. Tao, *Solid State Ionics* **2009**, *180*, 148 – 153; d) S. R. Phadke, C. R. Bowers, E. D. Wachsman, J. C. Nino, *Solid State Ionics* **2011**, *183*, 26 – 31; e) A. Tomita, N. Kajiyama, T. Kamiya, M. Nagao, T. Hibino, *J. Electrochem. Soc.* **2007**, *154*, B1265 – B1269; f) K. Genzaki, P. Heo, M. Sano, T. Hibino, *J. Electrochem. Soc.* **2009**, *156*, B806 – B810; g) X. Wu, A. Verma, K. Scott, *Fuel Cells* **2008**, *8*, 453 – 458; h) R. Lan, S. W. Tao, *J. Alloys Compd.* **2009**, *486*, 380 – 385; i) H. T. Wang, J. W. Liu, W. B. Wang, G. L. Ma, *J. Power Sources* **2010**, *195*, 5596 – 5600; j) J. Xiao, H. M. Zhang, Z. J. Yang, H. T. Wang, G. L. Ma, Z. F. Zhou, *J. Alloys Compd.* **2012**, *521*, 106 – 111.
[10] Y. C. Jin, Y. B. Shen, T. Hibino, *J. Mater. Chem.* **2010**, *20*, 6214 – 6217.
[11] R. D. Shannon, *Acta. Crystallogr.* **1976**, *32*, 751 – 767.
[12] B. L. Zhu, C. S. Xie, D. W. Zeng, W. L. Song, A. H. Wang, *Mater. Chem. Phys.* **2005**, *89*, 148 – 153.
[13] J. Sárkány, *Appl. Catal. A* **2002**, *229*, 291 – 312.
[14] K. N. Grew, W. K. S. Chiu, *J. Electrochem. Soc.* **2010**, *157*, B327 – B337.
[15] B. M. Lok, B. K. Marcus, C. L. Angell, *Zeolites* **1986**, *6*, 185 – 194.
[16] K. Tadanaga, Y. Furukawa, A. Hayashi, M. Tatsumisago, *Adv. Mater.* **2010**, *22*, 4401 – 4404.
[17] N. Bonanos, B. Ellis, K. S. Knight, M. N. Mahmood, *Solid State Ionics* **1989**, *35*, 179 – 188.